

Linmin ZHANG, Bin LIU, Juntao WEI, Xudong SONG, Yonghui BAI, Jiaofei WANG, Ying ZHOU, Huijun YANG, Guangsuo YU

Crystallization and viscosity-temperature characteristics during co-gasification of industrial sludge and coal

© Higher Education Press 2022

Abstract Co-gasification of industrial sludge (IS) and coal was an effective approach to achieve harmless and sustainable utilization of IS. The long-term and stable operation of a co-gasification largely depends on fluidity of coal-ash slag. Herein, the effects of IS addition on the crystallization and viscosity of Shuangmazao (SMZ) coal were investigated by means of high temperature stage coupled with an optical microscope (HTSOM), a scanning electron microscopy coupled with an energy dispersive X-ray spectrometry (SEM-EDS), X-ray diffraction (XRD), a Fourier transform infrared spectrometer (FTIR), and FactSage software. The results showed that when the proportion of IS was less than 60%, with the addition of IS, the slag existed in an amorphous form. This was due to the high content of SiO₂ and Al₂O₃ in SMZ ash and blended ash, which had a high glass-forming ability (GFA). The slag formed at a high temperature had a higher polymerization degree and viscosity, which led to a

decrease in the migration ability between ions, and ultimately made the slag difficult to crystallize during the cooling. When the proportion of IS was higher than 60%, the addition of IS increased the CaO and FeO content in the system. As network modifiers, CaO and FeO could provide O²⁻ at a high temperature, which reacted with silicate network structure and continuously destroyed the complexity of network structure, thus reducing the polymerization degree and viscosity of slag. At this time, the migration ability between ions was enhanced, and needle-shaped/rod-shaped crystals were precipitated during the cooling process. Finally, the viscosity calculated by simulation and Einstein-Roscoe empirical formula demonstrated that the addition of IS could significantly improve the fluidity of coal ash and meet the requirements of the liquid slag-tapping gasifier. The purpose of this work was to provide theoretical support for slag flow mechanisms during the gasifier slagging-tapping process and the resource treatment of industrial solid waste.

Received Sept. 1, 2021; accepted Jan. 12, 2022; online Mar. 20, 2022

Linmin ZHANG, Bin LIU, Xudong SONG (✉), Yonghui BAI, Jiaofei WANG

State Key Laboratory of High-efficiency Utilization of Coal and Green Chemical Engineering, College of Chemistry and Chemical Engineering, Ningxia University, Yinchuan 750021, China

E-mail: xdsong@nxu.edu.cn

Juntao WEI

Joint International Research Laboratory of Biomass Energy and Materials, Co-Innovation Center of Efficient Processing and Utilization of Forest Resources, College of Materials Science and Engineering, Nanjing Forestry University, Nanjing 210037, China

Ying ZHOU, Huijun YANG

Institute of Coal Chemical Industry Technology, Ningxia Coal Industry Co., Ltd., Yinchuan 750000, China

Guangsuo YU (✉)

State Key Laboratory of High-efficiency Utilization of Coal and Green Chemical Engineering, College of Chemistry and Chemical Engineering, Ningxia University, Yinchuan 750021, China; Institute of Clean Coal Technology, East China University of Science and Technology, Shanghai 200237, China

E-mail: gsyu@nxu.edu.cn

Keywords co-gasification, industrial sludge, crystallization, viscosity, mineral matter evolution

1 Introduction

Industrial sludge (IS), as a solid waste, contains a great deal of toxic inorganic and organic pollutants [1], which can pose a serious threat to human health and the environment when it is treated by landfilling or stacking. Therefore, the reasonable reuse of IS has attracted an increasing amount of attention. IS has a high volatile content and a low fixed carbon content. Therefore, IS is similar to biomass because it is not only a solid waste, but also an energy material [2,3]. The mixed heat treatment of solid waste and coal is an efficient approach (e.g., combustion, pyrolysis, and gasification) [4,5]. However, with the increasingly higher requirements of the government for environmental protection, the clean

and efficient utilization of coal resources is constantly putting forward higher requirements. The co-gasification of solid waste and coal is a promising method, which cannot only improve the slag-tapping performance of coal ash, but also reduce the damage to the environment [6]. Previous studies also prove that the co-gasification of IS and coal is an effective approach to achieve harmless and sustainable treatment of IS [7,8].

In the co-gasification process, organic matters are gasified into syngas, and inorganic minerals are transformed into liquid molten slag at high temperature, flowing out along the wall and entering the slag bath [9]. Generally, continuous and stable slag-tapping is a prerequisite for the normal operation of the gasifier [10]. The ash fusion temperatures (AFTs) and viscosity-temperature characteristics are the key parameters guiding the stable operation of the gasifier [11,12]. AFTs are the primary basis for coal blending and optimization of operating parameters [13–15]. The operating temperature of the gasifier is usually 50–200°C higher than the flow temperature (FT) to ensure complete melting and smooth discharge of minerals [16]. As another important parameter, the viscosity is usually required to be 2.5 – 25 Pa·s [17–19]. When the viscosity is below 2.5 Pa·s, the excessively flowing liquid slag can continually scour and erode the refractory brick wall; when the viscosity is above 25 Pa·s, the slag is difficult to be discharged, which can cause blockage of the slag outlet [20,21].

At present, the research on the co-gasification of IS and coal was principally focused on the ash melting behavior [22,23]. For example, Schwitalla et al. [24] investigated the slagging characteristics of lignite and its mixture with sludge. It was demonstrated that when the content of sludge ash was increased to 50% (mass percentage), FT could be significantly reduced. At the same time, it was found that the FactSage thermodynamic calculations were very consistent with the experimental ash melting behavior. Similarly, Folgueras et al. [25] studied the slagging behavior of three types of sludge on lignite and found that the addition of sludge could reduce the AFTs. Meanwhile, based on the ternary phase diagram of $\text{SiO}_2\text{-Al}_2\text{O}_3\text{-CaO}$, it was illustrated that most of the minerals in the mixed ash were located in the low temperature region and close to eutectics. In addition, Li et al. [26] researched the effects of industrial sludge on AFTs of three kinds of high-melting-point coal. It was considered that the addition of iron-bearing industrial sludge reacted with mullite in high-melting-point coal ash, and eventually transformed into low-melting-point hercynite. However, in some cases, the assessment method of AFTs was feasible [27,28]. However, in actual industrial gasification operation, for some coal, although the FT was lower than the operating temperature of the gasifier, the fluidity of molten slag was still very poor [29]. Therefore, to achieve the optimal slag-tapping conditions, it was quite necessary to consider the viscosity-temperature characteristic parameters during the co-gasification process [30].

However, up to the present, the research on co-gasification of industrial sludge and coal has mainly been focused on the ash melting characteristics, while little research has been conducted on the crystallization and viscosity-temperature characteristics. Since the ash melting characteristics and viscosity-temperature characteristics jointly guide the stable operation of gasifier, it is particularly important to study the viscosity-temperature characteristics in the process of co-gasification of IS and coal.

The co-gasification of IS and coal is an effective way to realize the harmless and sustainable utilization of industrial solid waste. During the co-gasification, the fluidity of molten slag is determined by both the melting and viscosity-temperature characteristics of the coal ash. However, the research on co-gasification of IS and coal are mainly focused on the ash melting characteristics, and few studies on the crystallization and viscosity-temperature characteristics are conducted. Therefore, the effect of industrial sludge addition on the crystallization and viscosity-temperature characteristics of Ningdong coal was studied in this work. XRD and FTIR were employed to characterize the mineral phase and slag structure. In addition, the crystal morphology was *in situ* observed by the HTSOM. Moreover, SEM-EDS was adopted for high resolution and element distribution characterization. Furthermore, the viscosity was calculated using the Einstein-Roscoe empirical formula and FactSage thermodynamic software. Collectively, the purpose of this study is to provide some insights for the resource treatment of industrial sludge, hoping to provide some theoretical support for the slag flow mechanism in the process of co-gasification of industrial sludge and coal to reduce the frequency of accidental shutdown of the gasifier.

2 Materials and methods

2.1 Materials

In this work, the Shuangmazao coal (SMZ) and industrial sludge (IS) provided by CHN Energy Ningxia Coal Industry Co., Ltd., were selected as raw materials. According to GB/T212-2008 and GB/T476-2001, proximate and ultimate analyses of these two raw materials were conducted, as listed in Tables 1 and 2. Ash samples were prepared in a muffle furnace at 815°C as per GB/T 1574-2007. The ash chemical compositions were determined by X-ray fluorescence spectrometer

Table 1 Proximate analysis of SMZ and IS

Sample	Proximate analysis (d)/% (mass percentage)		
	VM	FC	A
SMZ	27.14	54.52	18.34
IS	41.71	20.46	37.83

Notes: VM—volatile matter; FC—fixed carbon; d—dry basis.

Table 2 Ultimate analysis of SMZ and IS

Sample	Ultimate analysis (d)/% (mass percentage)					
	A	C	H	N	S	O*
SMZ	18.34	63.01	4.10	0.74	1.86	11.95
IS	37.83	14.28	7.91	1.80	1.72	36.46

Notes: d—dry basis; *—calculated by difference.

(PANalytical Axios; RIGAKU ZSX Priums), and the results were presented in **Table 3** where it could be seen that the SiO₂ and Al₂O₃ contents were higher in SMZ, while the CaO and Fe₂O₃ contents were higher in IS.

Table 3 Ash chemical compositions of SMZ and IS

Sample	Compositions/% (mass percentage)									
	SiO ₂	Al ₂ O ₃	Fe ₂ O ₃	CaO	Na ₂ O	K ₂ O	MgO	SO ₃	Others	B/A
SMZ	50.84	21.05	6.70	8.90	1.95	1.67	3.54	2.61	2.74	0.32
IS	33.12	13.82	12.51	21.08	6.17	1.05	4.94	4.89	2.42	0.97

Notes: B/A = (Fe₂O₃ + CaO + Na₂O + K₂O + MgO)/(SiO₂ + Al₂O₃) [31,32].

According to the GB/T219-2008 standard, the SDAF4000 automatic analyzer was applied to determine the ash fusion temperatures (AFTs) in a weakly reducing atmosphere (CO:CO₂ = 3:2, volumetric) and the results were tabulated in **Table 4** where almost no significant difference could be observed in AFTs between SMZ and IS.

Table 4 Ash fusion temperatures of SMZ and IS

Sample	Ash fusion temperatures/°C			
	DT	ST	HT	FT
SMZ	1190	1214	1219	1230
IS	1182	1220	1223	1228

Notes: DT—deformation temperature; ST—softening temperature; HT—hemispherical temperature; FT—flow temperature.

2.2 Ash samples preparation

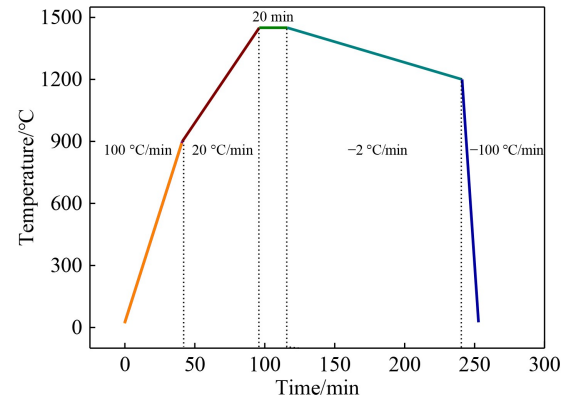
IS was added to the SMZ coal with mass fractions of 0, 20%, 40%, 60%, and 80% to prepare mixed samples, which were named IS0, IS2, IS4, IS6, and IS8, respectively (dimensionless parameter). Subsequently, the ash samples were prepared according to GB/T 1574-2007. First, the mixed sample was heated to 500°C within 30 min and kept for 30 min. Then, they were heated to 815°C and maintained for 2 h to ensure that the organic matter was fully oxidized.

2.3 Experimental methods

2.3.1 *In situ* crystallization observation using the HTSOM

A HTSOM (LINKAM TIS0500, England) was employed to *in situ* observe the crystal morphology variations during the cooling process. The temperature control procedure is exhibited in **Fig. 1**. The HTSOM equipment

and the specific operation process had been introduced in detail [14,19]. Moreover, each experiment was repeated at least three times for data accuracy.

**Fig. 1** Temperature program of HTSOM test.

2.3.2 XRD analysis

The ash samples were heated from room temperature to the target temperature and kept for 30 min to fully react in a weak reducing atmosphere. After that, the molten slag was quickly extracted and quenched in liquid nitrogen. Then, the quenched slag was ground and sieved to less than 200 μm for XRD analysis. The quenched slag samples were characterized by Bruker-AXS X-ray diffraction (XRD) with Cu Kα radiation (40 kV, 40 mA). The powder sample was placed on the sample stage and scanned in a step size of 0.02° within a 2θ range of 5° – 80°.

2.3.3 Thermodynamic calculation

The FactSage software package has been widely adopted to predict the ash fusion temperature and the slag viscosity [33]. In this work, using the FToxic and FactPS database, the main components of the ash samples (SiO₂, Al₂O₃, Fe₂O₃, CaO, Na₂O, and MgO) were selected in the Equilib module to calculate the minerals transformation behavior. The calculated temperature ranged from 1300 to 1600°C in steps of 50°C. By analyzing the minerals evolution, the contents of liquid phase and solid phase could be determined.

The Einstein-Roscoe empirical formula (Eq. (1)) was proverbially used in the calculation of the slag viscosity of solid-liquid mixed phase [34,35]. The liquid phase temperature (T_{liq} : the temperature at which the solid phase disappeared) was determined by the minerals evolution calculated by the Equilib module. Therefore, the calculation of the viscosity was divided into two cases: (1) When the temperature was higher than T_{liq} , the slag was pure liquid phase. At this time, the liquid phase composition and content calculated by Equilib were directly input into the viscosity module to calculate the viscosity of the sample higher than T_{liq} ; (2) when the

temperature was lower than T_{liq} , the slag was a solid-liquid mixed phase. Similarly, the Equilib module calculation results were used to determine the solid phase content and liquid phase composition and content in the molten slag, and then the corresponding liquid phase composition and content were input into the viscosity module to calculate the liquid phase viscosity. Finally, according to the solid content and liquid viscosity, the viscosity of the sample lower than T_{liq} was calculated by the Einstein-Roscoe empirical formula.

$$\begin{aligned} \text{Viscosity}_{(\text{solid+liquid mixture})} \\ = \text{Viscosity}_{(\text{liquid})}(1 - \text{solidfraction})^{-2.5}. \end{aligned} \quad (1)$$

2.3.4 Characterization of slag structure

The structure of quenched slag was characterized by using a Fourier transform infrared spectrometer (spectrum II, PerkinElmer, USA). The KBr drifts technique was used in the experiment. The powder sample was accurately mixed with KBr in a mass ratio of 1:200. The mixture was adequately grounded and then pressed into a thin tablet at 15 MPa. The spectral recording ranged from 400 to 4000 cm^{-1} , and the resolution was 0.4 cm^{-1} [36].

2.3.5 SEM-EDS analysis

The microstructure and elemental composition of the sputtered Au-Pd coating slag after the HTSOM test was determined by using a scanning electron microscopy (Talos-F200S) coupled with an energy dispersive X-ray

spectrometry (EDS) at an accelerating voltage of 10 kV. The elemental composition analysis was the result of point scanning on the crystal surface.

2.3.6 Viscosity measurement

The viscosity was measured by using a RV DVIII high temperature rotational viscometer in a mild reducing atmosphere ($\text{CO}_2:\text{CO} = 2:3$, volumetric). First, the pre-melted slag required to be prepared, which could be obtained by heating about 100 g ashes to 150°C higher than T_{liq} and maintaining it for 30 min to achieve equilibrium. After that, about 50 g pre-melted slags were crushed to 2 mm for viscosity testing. The apparatus was increasingly heated to 900°C at 15°C/min, then heated to 50°C higher than T_{liq} at 5°C/min, and the temperature was maintained for 30 min to obtain fully molten slag. Afterwards, the spindle was tardily immersed in the molten slag to start measuring the viscosity, and the cooling rate was 2°C/min. When the upper limit was exceeded, the viscometer stopped measuring.

3 Results and discussion

3.1 High-temperature crystallization

3.1.1 *In situ* crystallization morphology

The crystal morphological variations of different samples observed by the HTSOM are shown in Fig. 2 while a

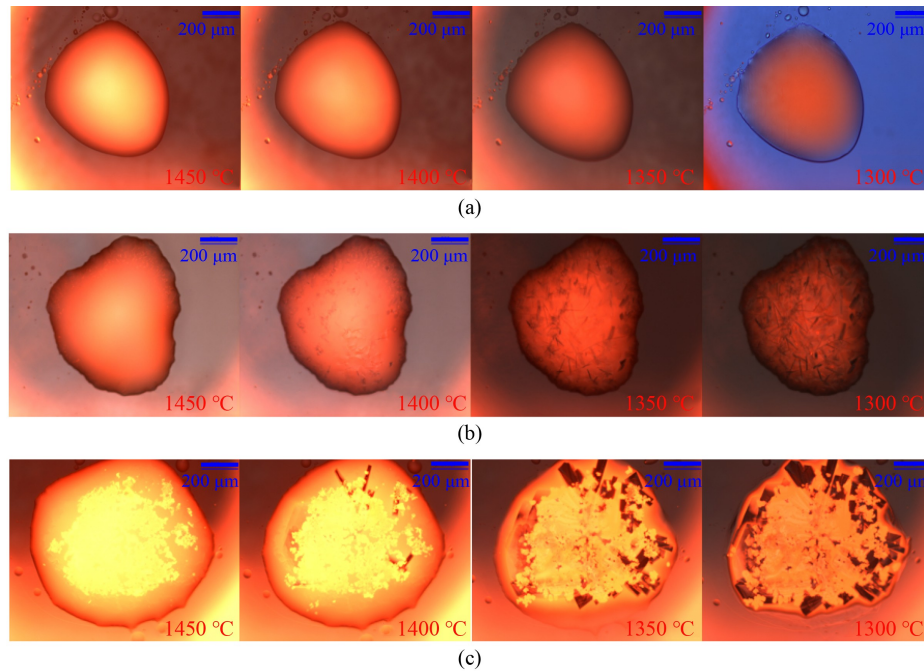


Fig. 2 Crystal morphological variations of different samples during cooling.
(a) IS4; (b) IS6; (c) IS8.

photograph taken with a projection light source when the sample is cooled to room temperature is displayed in Fig. 3, of which, Fig. 2(a) manifests the morphology change of IS4. It can be seen that IS4 shows a homogeneous melt and does not precipitate crystals during the cooling process, nor do IS0 and IS2 in the cooling process. Therefore, the crystal morphology of IS0 and IS2 is not exhibited. Meanwhile, it can be distinctly observed from Fig. 3(a) that when the molten slag is cooled to room temperature, the surface of the molten slag is in a uniform glass state. In this case, the crystallization may be completely inhibited due to the high glass-forming ability (GFA) of the IS0, IS2, and IS4 slag. This slag characteristic is usually related to the minimum cooling rate at which the glass phase is formed. Figure 2(b) shows the crystal morphology change of IS6 during the cooling process. The fine needle-shaped crystals are formed at 1400°C. With the decrease of temperature, needle-shaped crystals continue to grow, and the aspect ratio of needle-shaped crystals increase. Finally, the growth of crystal stops at 1300°C. The crystal morphology at room temperature is shown in Fig. 3(b), and the majority of fine needle-shaped crystals can be observed more clearly. Figure 2(c) shows the crystal morphology change of IS8 during the cooling process. It can be seen that rod-shaped crystals are precipitated first. As the temperature decreases, a large number of rod-shaped crystals are continuously precipitated, and the aspect ratio of rod-shaped crystals is also increased. Finally, the volume fraction and aspect ratio of the crystal do not change at about 1300°C. Meanwhile, the crystal morphology of IS8 at room temperature is exhibited in Fig. 3(c), and the majority of rod-shaped crystals can be observed. However, compared with the fine needle-shaped crystals precipitated by IS6, the aspect ratio of the crystals precipitated in the IS8 is much greater than that of IS6 during the cooling process. This indicates that IS8 has a high crystallization rate. Crystallization usually involves two stages, namely nucleation and crystal growth. The nucleation rate and the crystal growth rate affect the crystallization rate development, thereby affecting the change of the viscosity. The crystallization behavior of slag also affects crystallization kinetics. In the classical nucleation theory, the chemical potentials and interface energy of the solid-liquid phase determine the nucleation rate of the solid-phase nuclei precipitated.

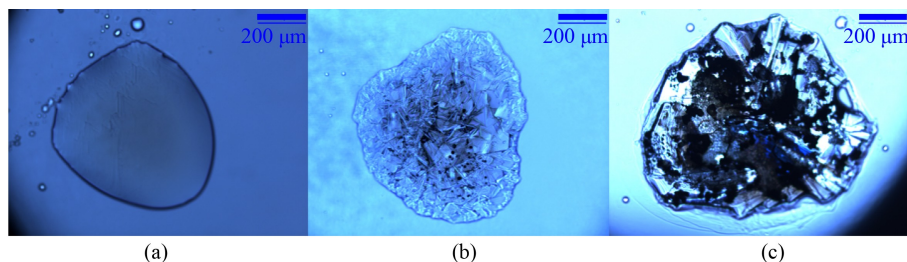


Fig. 3 Crystal morphology at room temperature.
(a) IS4; (b) IS6; (c) IS8.

3.1.2 Surface morphology characterization via SEM

To more intuitively observe the effect of IS additive on the crystal morphology of the SMZ coal, SEM was used to perform high-resolution characterization of the samples after the HTSOM experiment, and the results were shown in Figs. 4(a)–4(c). At the same time, the surface elements were investigated with an energy spectrometer (Fig. 4(d)). It can be seen from Fig. 4(a) that the slag of IS4 is a homogeneous melt without crystal precipitation. The reason for this is that when the addition proportion of IS is low (IS0-IS4), the content of CaO in the ash is low while SiO₂ and Al₂O₃ are high, which makes the slag have a high glass forming ability (GFA), thus inhibiting the formation of crystals and existing in the form of glass. It is observed from Fig. 4(b) that there are a large number of fine needle-shaped crystals on the molten slag surface. Figure 4(c) is the morphology of the SEM image of IS8 crystal. It can be seen that the molten slag appears to be in the form of rod-shaped crystals. The element distribution results of crystals in IS6 and IS8 are shown in Fig. 4(d). The main elements that form crystals are Si, Al, Ca, and O, with Fe and Mg rarely involved. The ratio of Si:Al:Ca is about 2:2:1, which is the same as the chemical composition of anorthite. The reason for this is that, with the addition of IS, the content of CaO in blended ash increases. The increased CaO content could react with SiO₂ and Al₂O₃ in the ash, causing the slag to precipitate anorthite crystals driven by the temperature difference ($2\text{SiO}_2 + \text{Al}_2\text{O}_3 + \text{CaO} \rightarrow \text{CaAl}_2\text{Si}_2\text{O}_8$). However, compared to IS6 (needle-like), the IS8 (rod-shaped) crystals have a larger aspect ratio, which indicates that the crystal growth of IS8 is more sufficient during the cooling process.

3.2 Mineral analyses

3.2.1 Raw ash mineral analysis

The mineral components of the SMZ coal ash and the IS ash prepared at 815°C are shown in Fig. 5 where it can be seen that the mineral components of the SMZ coal ash are

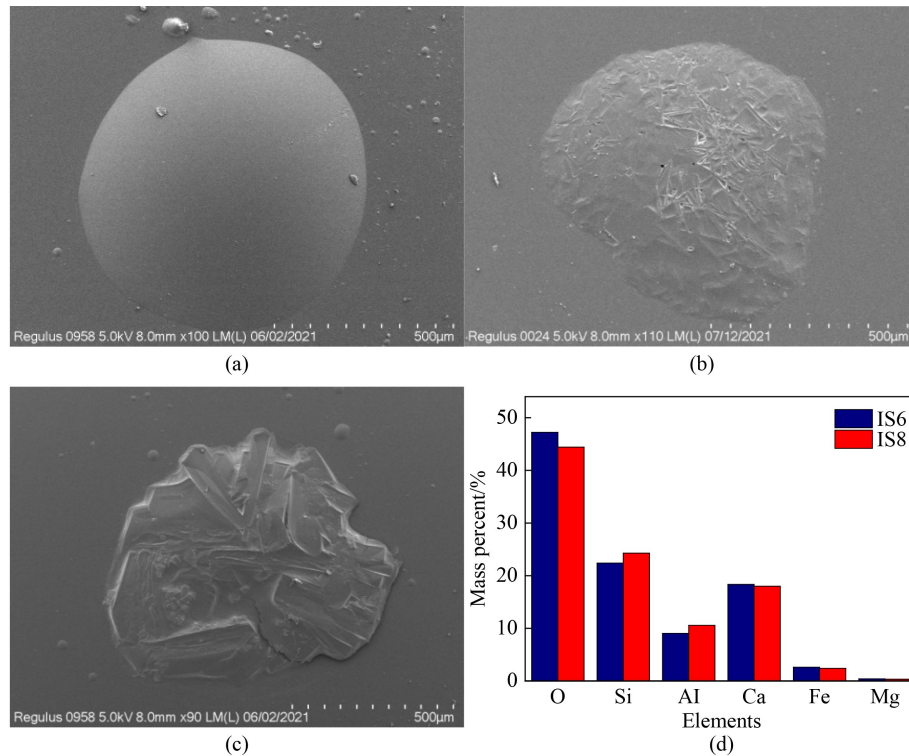


Fig. 4 SEM-EDS results of quenched slag.

(a) IS4; (b) IS6; (c) IS8; (d) elemental analysis.

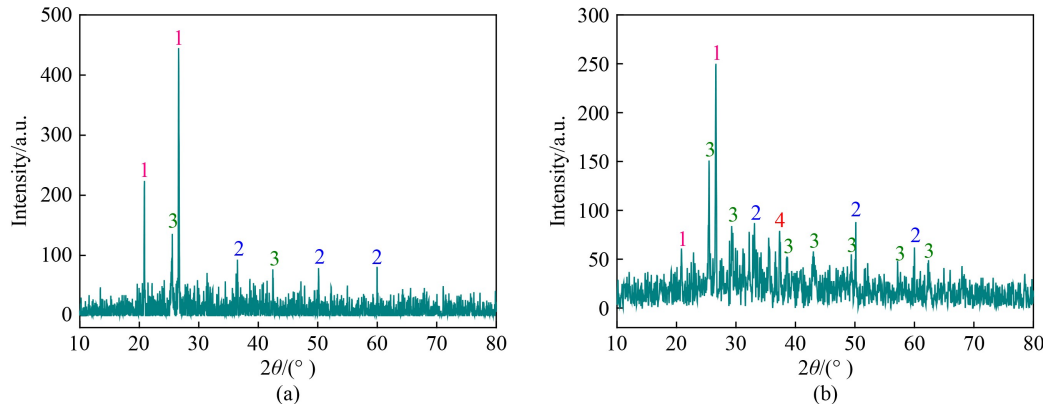


Fig. 5 XRD patterns of raw ashes (1—Quartz (SiO_2), 2—Hematite (Fe_2O_3), 3—Anhydrite (CaSO_4), 4—Lime (CaO)).
 (a) SMZ ash; (b) IS ash.

quartz (SiO_2), hematite (Fe_2O_3), and anhydrite (CaSO_4), among which quartz has the strongest diffraction peak. In addition, since the diffraction intensity of minerals is proportional to its content [36], the main mineral in the SMZ coal ash is quartz. The mineral components of the IS ash are quartz (SiO_2), hematite (Fe_2O_3), anhydrite (CaSO_4), and lime (CaO). Compared with the SMZ coal ash, the content of the quartz of the IS ash is significantly reduced while that of hematite and anhydrite is increased, and a new mineral lime (CaO) has appeared. Therefore, the IS ash is rich in calcium and iron.

3.2.2 Influence of IS addition on mineral evolution

Figure 6 shows the XRD patterns of samples with different IS proportions quenched at 1350°C. It can be seen that for IS0, IS2, and IS4, the quenched slag exists in an amorphous form. For IS6 and IS8, many strong diffraction peaks are observed in the XRD patterns. After matching, these substances are identified as anorthite, which also indicates that anorthite is the main component in the large number of fine needle-shaped crystals and rod-shaped crystals observed by the HTSOM. Moreover, IS8 exhibits more and stronger anorthite diffraction

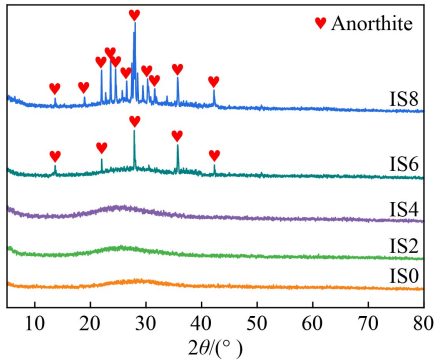


Fig. 6 XRD patterns of samples with different IS proportion quenched at 1350°C.

peaks than IS6. It was reported that the diffraction intensity was proportional to the content for the same substance [37]. In other words, the content of anorthite precipitated in IS8 is higher than that in IS6 during the cooling process. This is consistent with the *in situ* observation results of the HTSOM. The volume fraction and aspect ratio of IS8 crystals precipitated in the cooling process are much larger than those of IS6.

3.3 Influence of IS addition on molten slag structure

FTIR spectra were adopted to characterize the

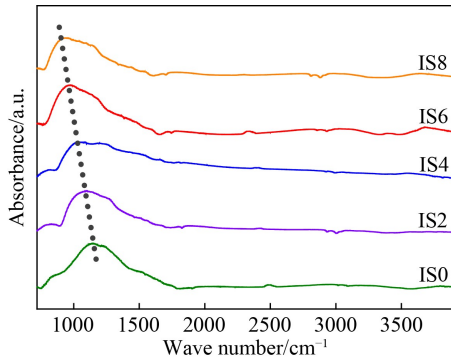


Fig. 7 FTIR spectra of quenched slag with different IS proportions.

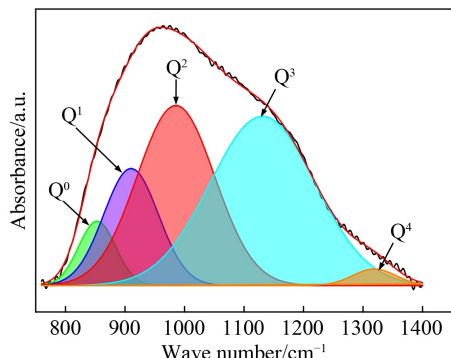


Fig. 8 A typical deconvolution of FTIR spectra.

microstructure information of different slag samples. The FTIR results and typical deconvolution of the FTIR spectra are shown in Figs. 7 and 8. It was accepted that the FTIR spectra of silicate slag were focused in the wavenumber region between 800 and 1200 cm⁻¹, which was related to the symmetric stretching vibration of [SiO₄] tetrahedron [38]. The characteristic stretching vibration of the SiO₄ tetrahedron was distinguished by introducing the Qⁿ unit, where the index n was the amount of Si-O-Si bridging oxygen and represented the molten slag polymerization degree. The index “n” was defined as a different microstructure from 0 to 4. For example, Q⁰ existed as a monomer such as [SiO₄]⁴⁻ (related to 850 – 880 cm⁻¹), Q¹ was indicated as a dimer structure like [Si₂O₇]⁶⁻ (related to 900 – 920 cm⁻¹), Q² represented a chain structure such as [SiO₃]²⁻ (related to 950 – 1000 cm⁻¹), Q³ was a planar layered structure like [Si₂O₅]²⁻ (related to 1050 – 1100 cm⁻¹), and Q⁴ was the three-dimensional network structure like SiO₂ (related to 1060 – 1200 cm⁻¹) [39]. Therefore, the higher n value represents a higher polymerization degree of silicate slag and a stronger aluminosilicate skeleton. As presented in Fig. 7, from ISO to IS8, the peak shifts to a low wave number, which indicates that the addition of IS can reduce the molten slag polymerization degree.

Figure 9 exhibits the quantitative results of Qⁿ units of different slag samples. As can be observed from Fig. 9, with the increase of IS proportion, the contents of Q⁰, Q¹, and Q² increase in varying degrees. On the contrary, the contents of Q³ and Q⁴ decrease to different degrees, and the reduction of Q³ is the most significant. Therefore, the variation of the Qⁿ unit content suggests that the polymerization degree of high temperature slag decreases continuously with the increase of the IS content. This is due to the relatively high content of SiO₂ and Al₂O₃ for SMZ. According to the network structure theory, SiO₂ and Al₂O₃ components can form a tetrahedron and become the basic units in the silicate network structure at a high temperature. With the increase of the SiO₂ and Al₂O₃ content, the network structure becomes more complex and polymerized. However, IS had a higher content of alkaline oxides, and Fe²⁺ and Ca²⁺ could be connected with the unsaturated O²⁻ in the silicate

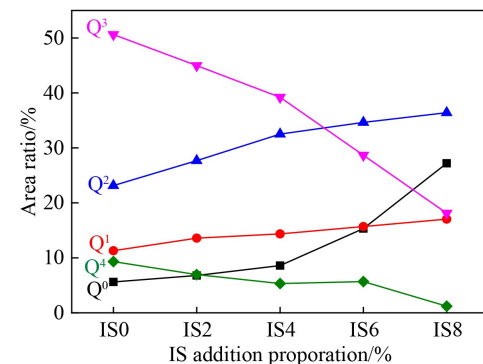


Fig. 9 Qⁿ unit contents based on deconvolution results.

network structure to destroy the network structure [40,41]. Moreover, with the increase of the alkaline oxide content, more unsaturated O^{2-} can be obtained from the silicate network structure, which destroys the network structure complexity and makes the network structure smaller.

Here, the difference of *in situ* crystallization morphology of different samples could be well explained by the variation of molten slag polymerization degree. For IS0, IS2, and IS4, the molten slag polymerization degree is high and leads to a weak interionic migration, which was ultimately not conducive to the formation of crystal nucleus and crystal growth. However, for IS6 and IS8, fine needle-shaped and rod-shaped crystals are precipitated during the cooling process. The reason for this is that the molten slag polymerization degree decreases continuously with the increase of IS proportion. As a result, the migration ability between ions is enhanced driven by the temperature difference, which contributes to the formation of crystal nucleus and the growth of crystal. In addition, since the polymerization degree of IS8 is lower than that of IS6, the volume fraction and aspect ratio of IS8 are much larger than those of IS6. Therefore, the evolution of microstructure can be well related to the variation of crystal morphology.

3.4 Viscosity-temperature curves

Kondratiev and Ilyushechkin [42] and Ge et al. [43] investigated the effect of solid volume fraction and morphology in molten slag on viscosity, and explained that crystal morphology (e.g., the size and shape) had a great effect on viscosity. Therefore, to better expound the influence of molten slag microstructure on the viscosity-temperature characteristics, the viscosity of different samples at 1300 – 1600°C was calculated by FactSage software in combination with the Einstein-Roscoe empirical formula, as shown in Fig. 10(a). Meanwhile, a group of sample was selected to compare the viscosity measured by the experiment and the viscosity calculated by the simulation (e.g., IS4). It can be seen from Fig. 10(b)

that there is still a certain deviation between the simulated viscosity and the actual viscosity. This may be caused by the fact that the calculation method of FactSage simulation software is the global equilibrium analysis [42,44]. However, under actual operating conditions, the overall state of the gasifier may deviate far away from the theoretical global equilibrium. Therefore, there is some deviation between the actual viscosity and the simulated viscosity. Nevertheless, the viscosity calculated by FactSage simulation is still instructive.

In the simulation, $Fe^{2+}/Fe^{3+} = 8:2$ (mass ratio) was set to eliminate the influence of atmosphere on the Fe valence state [38]. Moreover, it can be seen from Table 3 that the S/A of SMZ coal is so close to that of IS that the effect of S/A on crystallization and viscosity could be eliminated [45]. It can be seen from the results that the viscosity increases with the decrease of temperature. With the increase of IS proportion, the viscosity rise rate declines constantly. Therefore, the addition of IS can significantly reduce the slag viscosity. In combination with the influence of IS addition on crystal morphology, molten slag structure and viscosity, it can be seen that the slag with a high polymerization degree exhibits a higher viscosity, which limits the ion migration ability in the liquid molten slag and ultimately makes the slag difficult to crystallize. Conversely, the slag with low polymerization degrees exhibits a lower viscosity, which enhances the ion migration ability in the slag, and eventually contributes to the formation of crystal nucleus and the growth of crystal.

Generally, to guarantee the normal slag-tapping of the gasifier, the viscosity at the operating temperature required is between 2.5 and 25 Pa·s (shaded in Fig. 10(a)) [17]. In addition, it was reported that the operating temperature of the gasifier should be about 150 – 200°C higher than the FT of coal ash [38]. Therefore, according to Table 4, the operating temperature of the gasifier should reach at least about 1400°C to insure normal liquid slag-tapping [46,47]. For IS0, IS2, and IS4, the

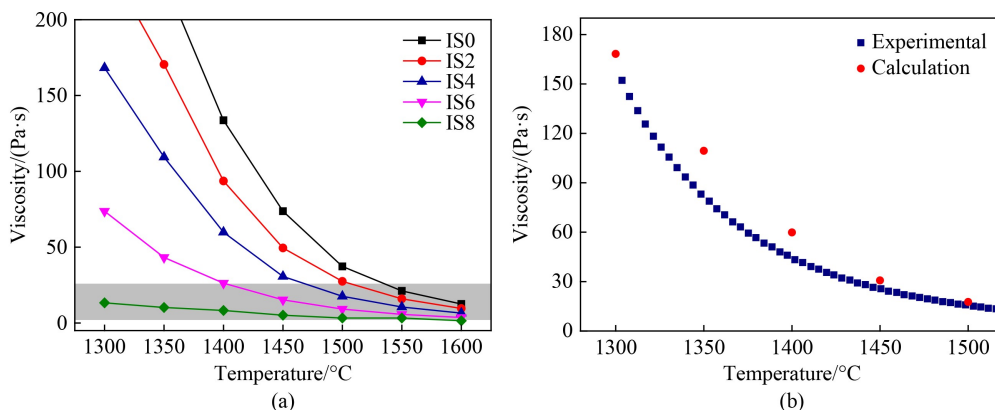


Fig. 10 Viscosity-temperature curves of mixed samples with different IS proportions. (a) Calculated by simulation; (b) comparison of calculation and experimental.

excessive viscosity at the operating temperature will lead to blockage of the slag-tapping outlet; otherwise, a higher temperature was required to ensure normal slag-tapping, which will significantly increase energy consumption. However, for IS8, too low a viscosity could make the fluidity of liquid slag too strong, which could accelerate the erosion and the fall off of refractory bricks [19,48]. The above analysis indicates that IS6 is more suitable. Therefore, the co-gasification of IS with appropriate proportion and coal was an effective method, which could not only realize the resource utilization of solid waste, but also ensure a lower operating temperature and avoid the slag-tapping problems.

4 Conclusions

The effects of IS addition on the crystallization and viscosity of Shuangmazao (SMZ) coal were investigated by means of HTSOM, a SEM-EDS, XRD, a FTIR, and FactSage software. Based on the experiment, it can be concluded that due to the high content of SiO_2 and Al_2O_3 in the SMZ coal ash, the slag with a complex network structure is formed at high temperatures, which leads to the weakening of the migration ability between ions. The SMZ coal ash does not precipitate any crystals during cooling.

IS6 and IS8 precipitate fine needle-shaped crystals and rod-shaped crystals respectively during the cooling process, which are matched to anorthite. The reason for this is that the addition of IS with the high basic oxides (CaO and Fe_2O_3) can connect with the unsaturated O^{2-} in the silicate network structure, which destroys the complex network structure and reduces the polymerization degree of the molten slag. The reduction of the slag polymerization degree enhances the ion mobility, which is beneficial to the formation of crystal nucleus and the growth of crystals.

According to the crystal morphology of IS6 and IS8, because the slag polymerization degree of IS8 is relatively low and the crystals are easy to grow, the aspect ratio of the crystals precipitated by IS8 is larger than that of IS6.

The calculation of viscosity by FactSage thermodynamics software suggests that IS additive could significantly reduce the viscosity to meet the requirements of liquid slag-tapping gasifiers.

Acknowledgments This work was supported by the project of Key Research Plan of Ningxia (2019BEB04030 and 2019BCH01001), and the project of CHN Energy Ningxia Coal Industry Co., Ltd. (NXMY2112).

Notations

AFTs	Ash fusion temperatures
B/A	Ratio of basic to acid
S/A	Ratio of silicon to aluminum
DT	Deformation temperature

ST	Softening temperature
HT	Hemispherical temperature
FT	Flow temperature
GFA	Glass-forming ability
T_{liq}	Liquid temperature
HTSOM	High temperature stage coupled with optical microscope system
SEM-EDS	Scanning electron microscopy coupled with energy dispersive X-ray spectrometry
XRD	X-ray diffraction
FTIR	Fourier transform infrared spectrometer
SMZ	Shuangmazao coal
IS	Industrial sludge
IS0	0 wt% IS addition to SMZ coal
IS2	20 wt% IS addition to SMZ coal
IS4	40 wt% IS addition to SMZ coal
IS6	60 wt% IS addition to SMZ coal
IS8	80 wt% IS addition to SMZ coal
Q^0	$[\text{SiO}_4]^{4-}$ monomer structure
Q^1	$[\text{Si}_2\text{O}_7]^{6-}$ dimer structure
Q^2	$[\text{SiO}_3]^{2-}$ chain structure
Q^3	$[\text{Si}_2\text{O}_5]^{2-}$ planar layered structure
Q^4	SiO_2 three-dimensional network structure

References

- Rulkens W. Sewage sludge as a biomass resource for the production of energy: overview and assessment of the various options. *Energy & Fuels*, 2008, 22(1): 9–15
- Goswami R, Das R. Waste heat recovery from a biomass heat engine for thermoelectric power generation using two-phase thermosyphons. *Renewable Energy*, 2020, 148: 1280–1291
- Goswami R, Das R. Energy cogeneration study of red mulberry (*Morus rubra*)-based biomass. *Energy Sources. Part A, Recovery, Utilization, and Environmental Effects*, 2020, 42(8): 979–1000
- Kijo-Kleczkowska A, Środa K, Kosowska-Golachowska M, et al. Experimental research of sewage sludge with coal and biomass co-combustion, in pellet form. *Waste Management (New York, N.Y.)*, 2016, 53: 165–181
- Deng N, Li D Y, Zhang Q, et al. Simulation analysis of municipal solid waste pyrolysis and gasification based on Aspen plus. *Frontiers in Energy*, 2019, 13(1): 64–70
- Yue G, Lyu J, Li S. Clean and highly-efficient utilization of coal. *Frontiers in Energy*, 2021, 15(1): 1–3
- Wang L, Skjervik G, Hustad J E, et al. Sintering characteristics of sewage sludge ashes at elevated temperature. *Fuel Processing Technology*, 2012, 96: 88–97
- Folgueras M B, Alonso M, Folgueras J R. Effect of sludge addition to coal on Na, K and S volatilisation in ashing process and ash fusibility. *Fuel Processing Technology*, 2015, 138: 714–723
- Stickler D B, Gannon R E. Slag-coated wall structure technology

- for entrained flow gasifiers. *Fuel Processing Technology*, 1983, 7(3): 225–238
- 10. Alam M T, Dai B, Wu X, et al. A critical review of ash slagging mechanisms and viscosity measurement for low-rank coal and bio-slags. *Frontiers in Energy*, 2021, 15(1): 46–67
 - 11. Xue Z, Guo Q, Gong Y, et al. *In-situ* atomization and flame characteristics of coal water slurry in an impinging entrained-flow gasifier. *Chemical Engineering Science*, 2018, 190: 248–259
 - 12. Yan T, Bai J, Kong L, et al. Effect of $\text{SiO}_2/\text{Al}_2\text{O}_3$ on fusion behavior of coal ash at high temperature. *Fuel*, 2017, 193: 275–283
 - 13. Link S, Yrjas P, Hupa L. Ash melting behaviour of wheat straw blends with wood and reed. *Renewable Energy*, 2018, 124: 11–20
 - 14. Zhang L, Wang J, Song X, et al. Influence of biomass ash additive on fusion characteristics of high-silicon-aluminum coal ash. *Fuel*, 2020, 282: 118876
 - 15. Wang J, Liu X, Guo Q, et al. Application of biomass leachate in regulating the fusibility of coal ash. *Fuel*, 2020, 268: 117338
 - 16. Ninomiya Y, Sato A. Ash melting behavior under coal gasification conditions. *Energy Conversion and Management*, 1997, 38(10-13): 1405–1412
 - 17. Hsieh P Y. Viscous deformation as a measure of heat work during coal ash fusibility testing. *Fuel*, 2020, 281: 118723
 - 18. Bryant G W, Lucas J A, Gupta S K, et al. Use of thermomechanical analysis to quantify the flux additions necessary for slag flow in slagging gasifiers fired with coal. *Energy & Fuels*, 1998, 12(2): 257–261
 - 19. Zhang L, Wei J, Wang J, et al. Deep insight into the ash fusibility and viscosity fluctuation behavior during co-gasification of coal and indirect coal liquefaction residue. *Fuel*, 2021, 305: 121620
 - 20. Cao X, Kong L, Bai J, et al. Influence of water vapor on continuous cooling crystallization characteristics of coal ash slag. *Fuel*, 2021, 303: 121241
 - 21. He C, Bai J, Kong L, et al. Effects of atmosphere on the oxidation state of iron and viscosity behavior of coal ash slag. *Fuel*, 2019, 243: 41–51
 - 22. Li F, Zhao C, Li J, et al. Investigation on ash fusion behavior modification of wheat straw by sludge addition. *Journal of the Energy Institute*, 2021, 98: 1–10
 - 23. Li W, Li M, Li W, et al. Study on the ash fusion temperatures of coal and sewage sludge mixtures. *Fuel*, 2010, 89(7): 1566–1572
 - 24. Schwitalla D, Reimöller M, Forman C, et al. Ash and slag properties for co-gasification of sewage sludge and coal: an experimentally validated modeling approach. *Fuel Processing Technology*, 2018, 175: 1–9
 - 25. Folgueras M B, Alonso M, Folgueras J R. Modification of lignite ash fusion temperatures by the addition of different types of sewage sludge. *Fuel Processing Technology*, 2015, 131: 348–355
 - 26. Li M, Li F, Liu Q, et al. Regulation of ash fusibility for high ash-fusion-temperature (AFT) coal by industrial sludge addition. *Fuel*, 2019, 244: 91–103
 - 27. Wall T F, Creelman R A, Gupta R P, et al. Coal ash fusion temperatures-new characterization techniques, and implications for slagging and fouling. *Progress in Energy and Combustion Science*, 1998, 24(4): 345–353
 - 28. Gong X, Lu W, Guo X, et al. Pilot-scale comparison investigation of different entrained-flow gasification technologies and prediction on industrial-scale gasification performance. *Fuel*, 2014, 129: 37–44
 - 29. van Dyk J C, Waanders F B, Benson S A, et al. Viscosity predictions of the slag composition of gasified coal, utilizing FactSage equilibrium modelling. *Fuel*, 2009, 88(1): 67–74
 - 30. Safronov D, Förster T, Schwitalla D, et al. Numerical study on entrained-flow gasification performance using combined slag model and experimental characterization of slag properties. *Fuel Processing Technology*, 2017, 161: 62–75
 - 31. Miguez J L, Porteiro J, Behrendt F, et al. Review of the use of additives to mitigate operational problems associated with the combustion of biomass with high content in ash-forming species. *Renewable & Sustainable Energy Reviews*, 2021, 141: 110502
 - 32. Wang Y, Li L, An Q, et al. Investigation on ash fusion temperature and slagging characteristic of Zhundong coal blends, part 1: the effect of two solid wastes from calcium carbide production. *Fuel Processing Technology*, 2022, 228: 107138
 - 33. Wu G, Seibold S, Yazhenskikh E, et al. Viscosity model for oxide melts relevant to fuel slags. Part 3: the iron oxide containing low order systems in the system $\text{SiO}_2\text{-Al}_2\text{O}_3\text{-CaO-MgO-Na}_2\text{O-K}_2\text{O-FeO-Fe}_2\text{O}_3$. *Fuel Processing Technology*, 2018, 171: 339–349
 - 34. Duchesne M A, Bronsch A M, Hughes R W, et al. Slag viscosity modeling toolbox. *Fuel*, 2013, 114: 38–43
 - 35. Zhou J, Shen Z, Liang Q, et al. A new prediction method for the viscosity of the molten coal slag. Part 2: the viscosity model of crystalline slag. *Fuel*, 2018, 220: 233–239
 - 36. Cao X, Kong L, Bai J, et al. Effect of water vapor on coal ash slag viscosity under gasification condition. *Fuel*, 2019, 237: 18–27
 - 37. Zhang L, Wang J, Wei J, et al. Synergistic effects of CaO and MgO on ash fusion characteristics in entrained-flow gasifier. *Energy & Fuels*, 2021, 35(1): 425–432
 - 38. Cao X, Peng B, Kong L, et al. Flow properties of ash and slag under co-gasification of coal and extract residue of direct coal liquefaction residue. *Fuel*, 2020, 264: 116850
 - 39. Xing X, Pang Z, Mo C, et al. Effect of MgO and BaO on viscosity and structure of blast furnace slag. *Journal of Non-Crystalline Solids*, 2020, 530: 119801
 - 40. Gao J, Wen G, Huang T, et al. Effects of the composition on the structure and viscosity of the CaO-SiO₂-based mold flux. *Journal of Non-Crystalline Solids*, 2016, 435: 33–39
 - 41. Chen X, Kong L, Bai J, et al. The key for sodium-rich coal utilization in entrained flow gasifier: the role of sodium on slag viscosity-temperature behavior at high temperatures. *Applied Energy*, 2017, 206: 1241–1249
 - 42. Kondratiev A, Ilyushechkin A. Flow behaviour of crystallising coal ash slags: shear viscosity, non-Newtonian flow and temperature of critical viscosity. *Fuel*, 2018, 224: 783–800
 - 43. Ge Z, Kong L, Bai J, et al. Crystallization kinetics and T_{CV} prediction of coal ash slag under slag tapping conditions in an entrained flow gasifier. *Fuel*, 2020, 272: 117723
 - 44. Frandsen F, Dam-Johansen K, Rasmussen P. Trace elements from combustion and gasification of coal—an equilibrium approach. *Progress in Energy and Combustion Science*, 1994, 20(2): 115–138

45. Xuan W, Whitty K J, Guan Q, et al. Influence of SiO₂/Al₂O₃ on crystallization characteristics of synthetic coal slags. *Fuel*, 2015, 144: 103–110
46. Zhou H, Xing Y, Zhou M. Effects of modified Kaolin adsorbents on sodium adsorption efficiency and ash fusion characteristics during Zhundong coal combustion. *Journal of the Energy Institute*, 2021, 97: 203–212
47. Xie L, Lv Y, Xu L. The influence of the high potassium biomass on the ash fusion characteristics of coal. *Journal of the Energy Institute*, 2021, 95: 52–60
48. Cao X, Kong L, Bai J, et al. Measurement and simulation of viscosity characteristics of coal ash slag under water vapor condition in coal gasification. *Fuel*, 2022, 308: 121882